JOURNAL OF SOLID STATE CHEMISTRY **128,** 102–108 (1997)
ARTICLE NO. SC967176

Iron Zircon Pigments Prepared by Pyrolysis of Aerosols

P. Tartaj, T. González-Carreño, C. J. Serna,[1] and M. Ocaña[2]

Instituto de Ciencia de Materiales de Madrid, C.S.I.C., Campus Universitario de Cantoblanco, 28049 Cantoblanco (Madrid), Spain

Received April 15, 1996; in revised form September 25, 1996; accepted September 26, 1996

A procedure for the synthesis of iron zircon pigments by pyrolysis of liquid aerosols is reported. This method produces amorphous spherical particles, with diameters ranging from 20 to 200 nm, that can be transformed into reddish iron zircon pigments by heating at lower temperature (1000–1200°C) than that required for pure zircon. The low formation temperature of iron-doped zircon is attributed to the formation of a solid solution between Fe^{3+} cations and tetragonal zirconia, which would favor the diffusion of species required for zircon formation. It was found that the reddish color in the iron zircon pigments is due to α-Fe_2O_3 particles encapsulated in the zircon matrix. © 1997 Academic Press

INTRODUCTION

Iron-doped zircon pigments are one of the most widely used zircon-based pigments. At the present time, they are prepared by the classical ceramic procedure with the addition of alkaline halides to reduce the temperature of pigment formation (1–4).

It has been amply reported that ceramic powders with controlled particle size and shape can be prepared by chemical reactions in aerosols (5–11). The main advantages of this method over the classical one are its simplicity (grinding is reduced or eliminated) and continuous character which is desirable for industrial purposes.

In this paper we report a procedure for the preparation of spherical particles of reddish iron–zircon pigments based on the pyrolysis of liquid aerosols produced by nebulization of methanolic solutions of silicon ethoxide, zirconium oxychloride, and iron nitrate. To elucidate the origin of the pigments color, the localization of the iron cations in the ceramic matrix was investigated. In addition, the iron concentration was systematically varied in order to analyze its effect on the optical properties of the pigments.

[1] To whom correspondence should be addressed.

[2] Present address: Instituto de Ciencia de Materiales de Sevilla, C.S.I.C.-Universidad de Sevilla, Avda. Reina Mercedes s/n, P.O. Box 1115, 41080 (Sevilla), Spain.

EXPERIMENTAL

Sample Preparation

The preparation of $ZrO_2 \cdot SiO_2$ spherical particles containing different amounts of iron(III) was carried out by pyrolysis of liquid aerosols using an apparatus previously described (9). Proper amounts ($Fe/ZrSiO_4$ = 5–40% molar) of Silicon ethoxide (TEOS, Fluka, 97%), zirconium oxychloride ($ZrOCl_2 \cdot 8H_2O$, Aldrich, 98%), and iron(III) nitrate ($Fe(NO_3)_3 \cdot 9H_2O$, Aldrich, 99%) were dissolved in methanol. This solution was atomized with air at a constant pressure (1.6 kg/cm^2), and the resulting liquid droplets were dried at 250°C. The so-generated solid particles were then decomposed in a second furnace kept at 500°C and finally collected using an electrostatic chamber. These powders were calcined during 8 h at constant temperature in platinum crucibles to produce the $Fe–ZrSiO_4$ pigments.

The commercial iron–zircon pigment was supplied by Ferro Enamel Española S.A.

Characterization

The particle size and shape of the powders were examined by transmission electron microscopy (TEM, JEOL 2000FX2). The size distribution was evaluated by measuring several hundreds of particles. Chemical composition of the powders (zirconium, silicon, and iron content) was determined by plasma emission (ICP, Perkin Elmer 5500). For that, 100 mg of sample was first fused at 1100°C with a $KNaCO_3$:$Na_2B_4O_7$ mixture and then extracted with a HCl solution.

Differential thermal (DTA) and thermogravimetric (TGA) analyses (STA 781) were registered in air atmosphere at a heating rate of 10°C/min. X-ray diffraction (Philips PW1710) using Cu$K\alpha$ radiation, and infrared spectroscopy (Nicolet 20SXC) were used for identification purposes. To record the infrared spectra, the powders were diluted in KBr.

The cell parameters of the powders were measured by Rietveld analysis of the X-ray diffraction data carried out using the FULLPROF program (12). The diffractograms were registered using Cu$K\alpha$ radiation between 10 and 120°

0022-4596/97 $25.00

(2θ) at intervals of 0.04° (2θ) with an accumulation time for interval of 20 s. A 1/2° divergence slit and a receiving slit of 0.05 mm were employed. In all experiments a silicon standard (20% by weight) was mechanically mixed with the pigment (13). The crystallographic data for $ZrSiO_4$, tetragonal ZrO_2, and silicon were taken from references 14, 15, and 16, respectively.

The isoelectric point (i.e.p.) of the solids was determined by measuring electrophoretic mobilities of aqueous dispersions as a function of pH at constant ionic strength (0.01 mol/dm^3 NaCl) in a Delsa Coulter 440 apparatus.

Lab parameters of the powders were measured using a Dr. Lange, LUCI 100 colorimeter. In this color system, L is the color lightness ($L = 0$ for black and 100 for white), a is the green(−)/red(+) axis, and b is blue(−)/yellow(+) axis. For measurements, 40 mg of pigment was dispersed in doubly distilled water and filtered through 0.22 μm Millipore filters, resulting in a thin layer with a pigment density of 6 mg/cm^2. A white tile ceramic having chromaticity coordinates ($x = 0.315$, $y = 0.335$) was used as reference standard. Before color measurements the calcined samples were washed with a 2 mol/dm^3 HCl hot solution. For such a purpose, a dispersion containing 200 mg of sample in 200 cm^3 of acid solution was stirred by 4 h, and then the solid was separated from the washing liquid by centrifugation. The amount of iron leached out by this procedure was determined as a difference between the iron content in the washed and unwashed pigments.

^{57}Fe Mössbauer spectra were collected at room temperature with a conventional spectrometer using a ^{57}Co/Rh source. All spectra were computer fitted to Lorentzian lines. In some experiments, a probability distribution of hyperfine fields was also used. The isomer shift (IS) parameter was referred to α-iron.

XPS spectra were obtained with a VG Escalab 220 model using the Al$K\alpha$ excitation source. Calibration of the spectra was done at the C1s peak of surface contamination taken at 284.6 eV.

A vibrating sample magnetometer (EG&G PARK 155) was used to measure the magnetization curves.

RESULTS AND DISCUSSION

Powder Characterization and Thermal Evolution

Most of the characterization data hereafter presented correspond to sample F20 ($Fe/ZrSiO_4 = 20\%$ molar, Table 1) chosen as a representative example. All other studied samples showed a similar behavior except when indicated. The as prepared powders were amorphous to X-ray diffraction being composed of spherical particles (Fig. 1), with diameter ranging from 20 to 200 nm. Their infrared spectrum (Fig. 2) shows a strong band at 1035 cm^{-1} due to the Si–O stretching mode (17), whose low frequency suggests a good mixing of the components inside the particles. The broad band at 470 cm^{-1} must contain both O–Si–O bending and Zr–O stretching modes (17, 18).

The thermal evolution of the initial particles was studied by TG and DTA analyses. In the temperature range between 25 and 600°C, DTA (Fig. 3) shows features associated to the elimination of adsorbed water- (100°C) and nitrogen-containing species (365°C) coming from the precursors. Three exothermic effects were observed at temperatures higher than 600°C which are important for the understanding of the pigment formation. According to X-ray diffraction

TABLE 1
Amount of Iron ($Fe/ZrSiO_4$) Leached out in the Washing Procedure and Retained in the $Fe–ZrSiO_4$ Pigments Heated at Different Temperatures

Sample	Raw (Zr/Si) (molar)	Raw Fe (% molar)	Temperature (°C)	Washed Fe (% molar)	Retained Fe (% molar)
F5	1·01	5	1100	0.6	4.4
			1200	0.6	4.4
			1300	0.8	4.2
F10	1.02	10	1000	0.7	9.3
			1100	1.0	9.0
			1200	1.1	8.9
			1300	1.5	8.5
F20	1.00	20	1000	1.6	18.4
			1100	1.9	18.1
			1200	3.0	17.0
			1300	3.8	16.2
F40	1.01	40	1000	4.1	35.9
			1100	6.2	33.8
			1200	7.3	32.7
			1300	7.9	32.1

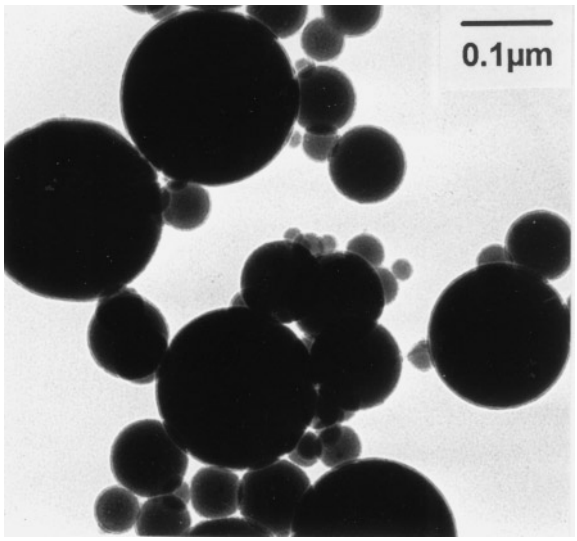

FIG. 1. TEM micrograph of sample F20 as prepared.

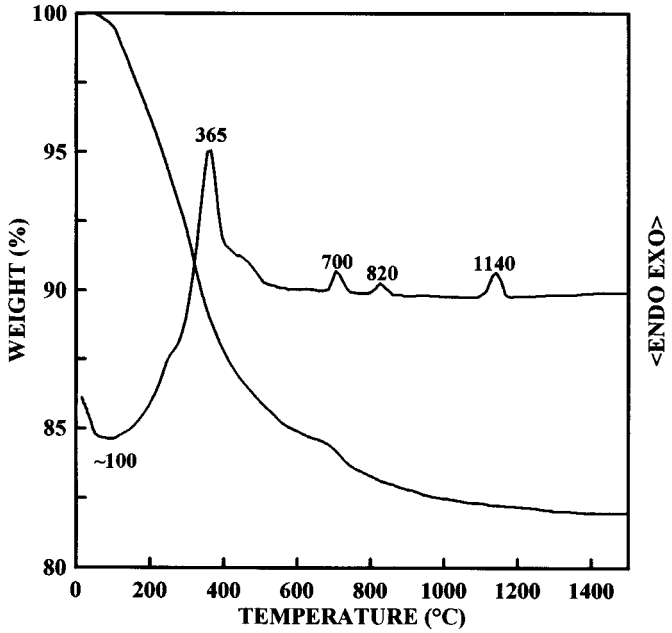

FIG. 3. Differential thermal and thermogravimetric curves obtained for sample F20.

(Fig. 4), the first (700°C) could be due to the crystallization of tetragonal or cubic zirconia (19, 20). The infrared spectrum of the sample heated at 700°C shows a band at $\sim 600\ cm^{-1}$ corresponding to tetragonal zirconia (18), indicating that the exothermic effect is associated to the crystallization of this phase. The exothermic peaks at 820 and 1140°C could be assigned to the crystallization of α-Fe_2O_3 and zircon, respectively, as suggested by X-ray diffraction

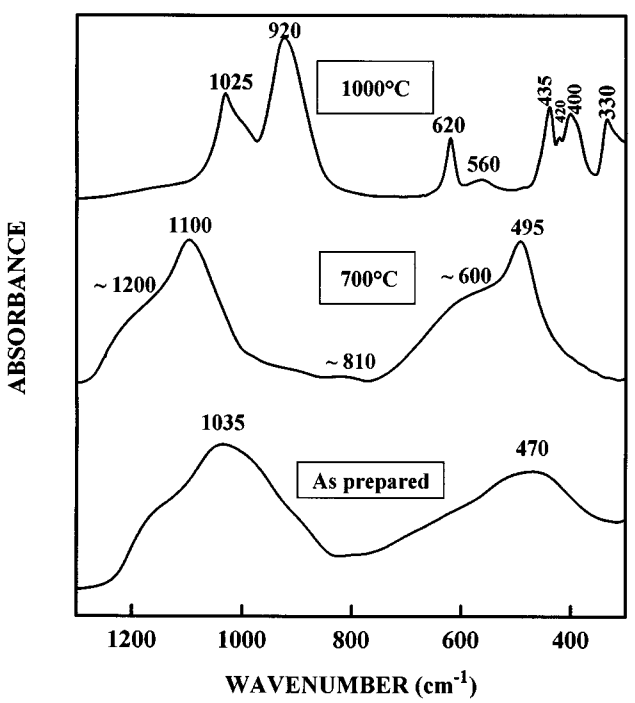

FIG. 2. Infrared spectra for sample F20 heated at different temperatures.

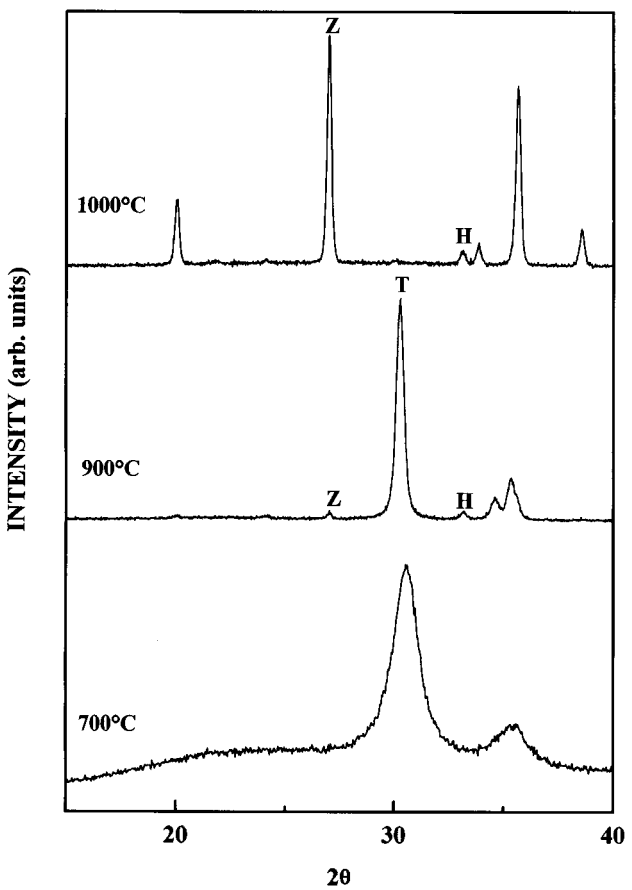

FIG. 4. X-ray diffraction patterns of sample F20 heated at different temperatures. The symbols represent T (tetragonal zirconia), Z (zircon), H (hematite), and C (cristobalite).

(Fig. 4). It must be pointed out that the temperatures of zircon formation decreases (from 1200 to 1140°C) with increasing the iron content (from 5 to 40% molar), suggesting a catalytic effect of iron or zircon crystallization.

The beginning of both zircon formation and hematite crystallization was detected by X-ray diffraction (Fig. 4) after heating at 900°C for 8 h on samples with iron content $\geq 10\%$ molar (F10, F20, and F40). At this temperature, X-ray diffraction clearly manifested the presence of tetragonal zirconia by the splitting of the peak at $2\theta \sim 35°$. In sample F5 (5% molar in iron), the onset of zircon formation was slightly retarded (1000°C) and the hematite phase was not detected probably due to its low concentration. Zircon formation was accomplished at 1000°C for samples F10, F20, and F40 and at 1100°C for sample F5. These temperatures are similar to that obtained when using the classical ceramic method in the presence of mineralizing agents (4), being significantly lower than that corresponding to undoped zircon prepared by a similar method (1400°C) (21). This behavior confirms the catalytic effect of iron on zircon crystallization.

The infrared spectra of sample F20 heated at increasing temperatures are shown in Fig. 2. At 700°C the spectrum shows the segregation of silica, as suggested by the shift of the Si–O stretching mode to higher frequencies (1100 cm^{-1}) (17). The appearance of bands at 1025, 920, 620, 435, 420, 400, and 330 cm^{-1} after calcining the sample at 1000°C indicates the presence of zircon (22), in agreement with X-ray diffraction (Fig. 4). It should be noted that the position of the bands shows some variations respect to previously reported spectra of zircon (7) which are due to differences in particle shape (22). At this temperature, the spectrum also displays a band at 560 cm^{-1}, whose intensity increased with iron content (data not shown), being assigned to hematite (23). The particles retained the initial spherical shape (Fig. 1) after zircon formation. However, interparticle sintering started with increasing temperature up to 1200°C and progressed on heating at 1300°C (data not shown).

Iron Content and Color in Iron Zircon Pigments

Table 1 shows the composition of the $Fe/ZrSiO_4$ samples heated at different temperatures above complete zircon crystallization ($\geqslant$1000°C), before and after leaching treatments. Although most of the initial iron amount ($> 80\%$) was retained in the pigments, a certain amount was leached out during the washing procedure, which increases with temperature and the iron raw content.

The evolution with temperature of the *Lab* parameters of the samples heated above zircon formation measured after leaching, is shown in Fig. 5. In all cases, these parameters correspond to a reddish color, the intensity of which increased (L decreased) with the iron content, whereas no significant variation was detected on heating a given sample at increasing temperature. The most striking changes with temperature and composition were observed for the a parameter whose maximum value (maximum red tint) was obtained at each temperature for sample F20. For a given iron content, the evolution of the a parameter with temperature, indicates a progressive change from red to black tint. A similar trend was observed for the b parameter with temperature, in agreement with the blackening of the pigments.

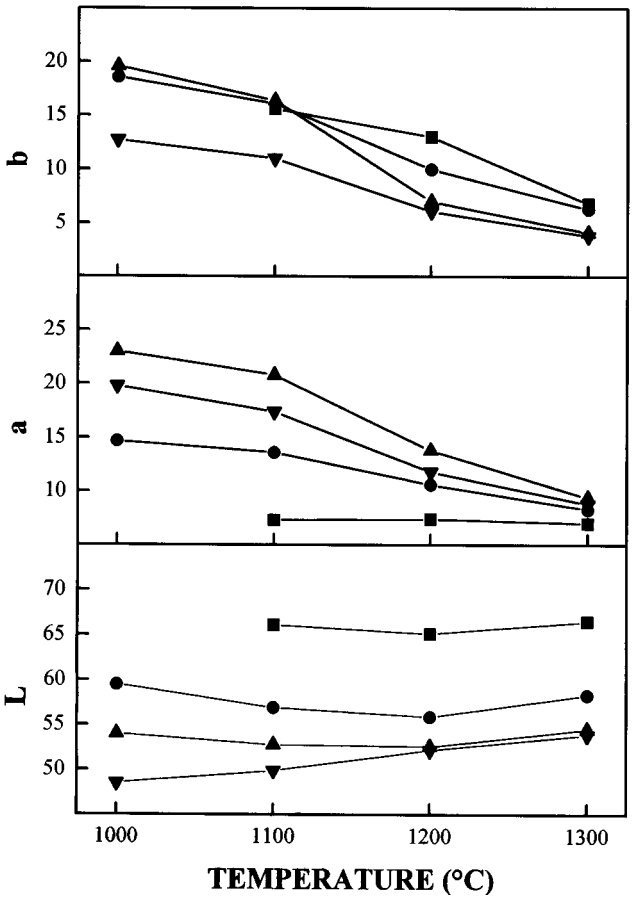

FIG. 5. *Lab* parameters obtained for sample F5 (■), F10 (●), F20 (▲), and F40 (▼) heated at different temperatures above zircon formation.

It should be noted that the *Lab* parameters of sample F20 heated at 1200°C and washed ($L = 52$, $a = 14$, and $b = 7$) are similar to those corresponding to a commercial iron–zircon pigment ($L = 4$, $a = 16$, and $b = 6$) although the former was prepared with lower iron content (sample F20, 20% molar, and commercial pigment, 50% molar) in the absence of mineralizers.

Formation Mechanism and Color Origin of Iron Zircon Pigments

In order to understand the catalytic effect of iron cations on zircon formation and the origin of the reddish color of

the pigments, a study of the localization of the iron cations in the ceramic matrix during calcination was carried out.

The unit cell parameters of the tetragonal zirconia phase present in sample F20 after heating at 900°C, just before of complete zircon formation (1000°C), are shown in Table 2, along with those obtained for a zirconia blank prepared under similar conditions. As observed, the unit cell volume of tetragonal zirconia is smaller than that of the blank, suggesting the formation of a solid solution between the iron cations and the zirconia lattice, in agreement with previous observations (24–26). This process must generate vacancies that would favor the zircon diffusionally limited nucleation (27), thus explaining the decrease in the temperature of zircon crystallization when compared with a pure zircon sample.

At 900°C, the room temperature (RT) Mössbauer spectrum (Fig. 6) consists of two magnetically split sextets and a doublet characteristics of high-spin Fe^{3+} ions. The parameters best fitting each signal are shown in Table 3. The sextet with $IS = 0.38\ mm \cdot s^{-1}$ and $QS = -0.21\ mm \cdot s^{-1}$ corresponds to α-Fe_2O_3 (28), in agreement with X-ray diffraction (Fig. 4). The parameters of the second sextet ($IS = 0.34\ mm \cdot s^{-1}$ and $QS = 0.0\ mm \cdot s^{-1}$) are in accordance with γ-Fe_2O_3 (29). The low value of the average hyperfine field ($H_A = 39.1T$) would be indicative of small particle size (30).

The doublet ($IS = 0.40\ mm \cdot s^{-1}$, $QS = 1.27\ mm \cdot s^{-1}$, and $\Gamma = 0.94\ mm \cdot s^{-1}$) may be assigned to the finest particles of γ-Fe_2O_3, in which the superparamagnetic relaxation produces a collapse of the magnetic hyperfine splitting. This signal could also have paramagnetic contributions due to the Fe^{3+} ions forming solid solutions with the zirconia lattice. The presence of γ-Fe_2O_3 was confirmed by measuring the magnetization curve (data not shown) which gave a saturation magnetization (60 ± 20 emu/g) in the range expected for this phase (31).

After zircon formation (1200°C), the only phase detected by Mössbauer spectroscopy in sample F20 was α-Fe_2O_3 (Fig. 6, Table 3). In addition, the variation in unit cell parameters measured under these conditions, respect to those of pure zircon (Table 2) are within the experimental error. These results suggest that zircon formation is accompanied by a thermally induced segregation of the Fe^{3+} ions from the zirconia lattice and the transformation of metastable γ-Fe_2O_3 phase into α-Fe_2O_3. Therefore, the only phase responsible of the reddish color of the iron–zircon pigments is α-Fe_2O_3. It must be pointed out the absence, in our Mössbauer spectrum, of a doublet, which has been recently reported for iron-doped zircon prepared by the classical ceramic method using mineralizers, and attributed to Fe^{3+} cations incorporated to the zircon lattice (4). However, the color is similar in both pigments, which confirms that the color properties are dominated by α-Fe_2O_3 (4).

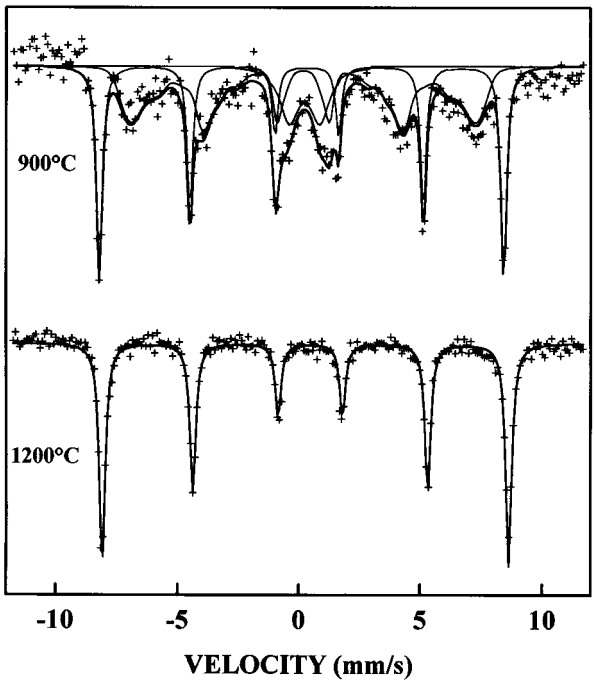

FIG. 6. Mössbauer spectra for sample F20 heated at 900 and 1200°C.

TABLE 2
Residual-Bragg Factor (R_b), Residual-Structure Factor (R_F), and Unit Cell Parameters Measured for Sample F20 Heated at 900 and 1200°C for a Zirconia Blank and for a Zircon Blank

Sample	F20 900 + [Silicon]	t-ZrO_2 + [Silicon]	F20 1200 + [Silicon]	$ZrSiO_4$ + [Silicon]
R_b	9.66 [10.6][a]	1.16 [5.38][a]	6.02 [3.60][a]	4.56 [8.52][a]
R_F	7.83 [7.10][a]	1.01 [4.38][a]	4.00 [3.28][a]	3.41 [5.93][a]
a (Å)	3.5971 (7)	3.6009 (5)	6.6049 (7)	6.6041 (7)
	[5.4308 (4)[a]]	[5.4310 (3)][a]	[5.4311 (3)][a]	[5.4307 (3)][a]
c (Å)	5.192 (1)	5.198 (1)	5.9797 (6)	5.9798 (6)
V (Å^3)	67.18 (4)	67.40 (3)	260.86 (6)	260.80 (8)

[a] Data refered to silicon standard having an a parameter of 5.4309 (15).

TABLE 3
Mössbauer Parameters for Sample F20 Heated at 900 and 1200°C

Signal	Mössbauer parameters	900°C	1200°C
Sextet	IS ($mm \cdot s^{-1}$)	0.38 ± 0.01	0.38 ± 0.01
	QS ($mm \cdot s^{-1}$)	-0.21 ± 0.01	-0.19 ± 0.01
	Γ ($mm \cdot s^{-1}$)	0.27 ± 0.01	0.31 ± 0.01
	H (T)	51.7 ± 0.1	52.1 ± 0.1
	A (%)	38 ± 2	100
Sextet	IS ($mm \cdot s^{-1}$)	0.34 ± 0.02	
	QS ($mm \cdot s^{-1}$)	0.00 ± 0.04	
	Γ ($mm \cdot s^{-1}$)	0.30	
	H_A (T)	39.1 ± 0.1	
	Γ_H	6.7 ± 0.5	
	A (%)	48 ± 11	
Doublet	IS ($mm \cdot s^{-1}$)	0.40 ± 0.04	
	QS ($mm \cdot s^{-1}$)	1.27 ± 0.06	
	Γ ($mm \cdot s^{-1}$)	0.94 ± 0.09	
	A (%)	14 ± 2	
	χ^2/degrees of freedom	1.6	2.4

Note. The symbols represent (IS) the isomer shift, (QS) the quadrupole splitting, (Γ) the width at height medium of signal, (H) the hyperfine field, (A) the relative iron amount of each phase and (χ^2/degrees of freedom) the goodness of fit.

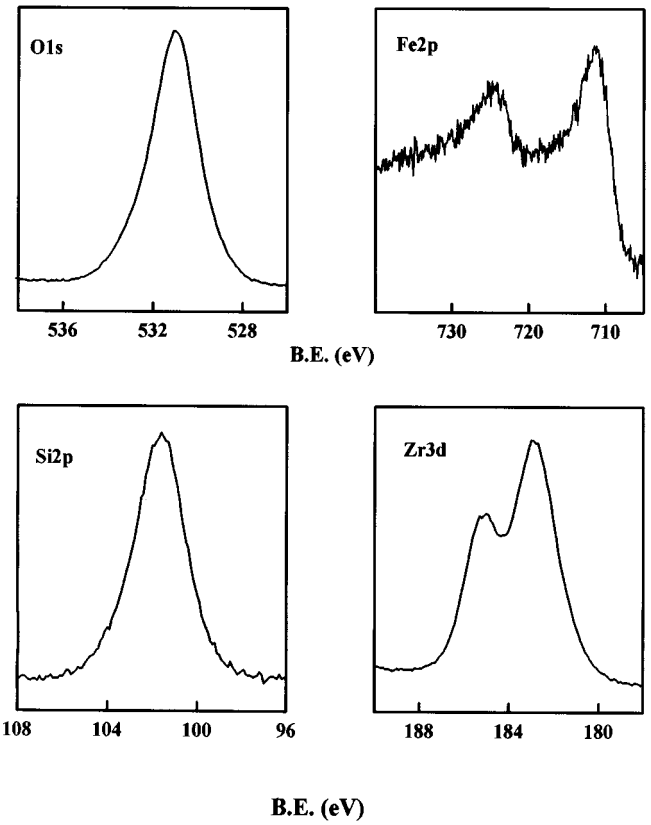

FIG. 7. XPS spectrum for sample F20 heated at 1200°C and leached.

In order to determine the localization of the α-Fe_2O_3 particles in the zircon matrix, the sample F20 heated at 1200°C and leached was examined by XPS spectroscopy (Fig. 7). As expected, the obtained spectrum showed peaks corresponding to the O_{1S} (531 eV), Si_{2p} (101.5 eV), $Zr_{3d_{5/2}}$ (182.8 eV), and $Zr_{3d_{3/2}}$ (185.1 eV) levels (32, 33). In addition, a doublet at 711.5–724.9 eV was detected which corresponds to the $Fe_{2p_{3/2}}$ and $Fe_{2p_{1/2}}$ levels in α-Fe_2O_3 (32), respectively. The $Fe/ZrSiO_4$ molar ratio calculated from these signals ($\sim 20\%$), similar to the average iron content in sample (Table 1), suggests that the α-Fe_2O_3 particles are homogeneously distributed in the zircon matrix. It should be noted that the Si/Zr ratio resulting from XPS spectrum is higher (Si/Zr = 1.7) than that determined by plasma emission (1.00), indicating an enrichment of silicon in the particles outlayers. In accordance with this, isoelectric points values (Fig. 8) (4.7–4.9) are lower than those reported for zircon (5.7) (34) and hematite (6–6.5) (35) which also manifests that silica is located at the particles surface, since the i.e.p. of this phase ranges between 1 and 3 (36). The presence of silica partially coating the pigment particles could be associated to an inhomogeneous precipitation process during aerosol drying as a consequence of the differences in solubility of TEOS, zirconium oxychloride and iron(III) nitrate (8).

Finally, the darkening of the iron zircon pigments when heating at a higher temperature (1300°C) (Fig. 5) can be related to an increase of the size of α-Fe_2O_3 particles since it is well-known that this oxide becomes progressively achromatic (*a* and *b* approach zero) with increasing particle size (37).

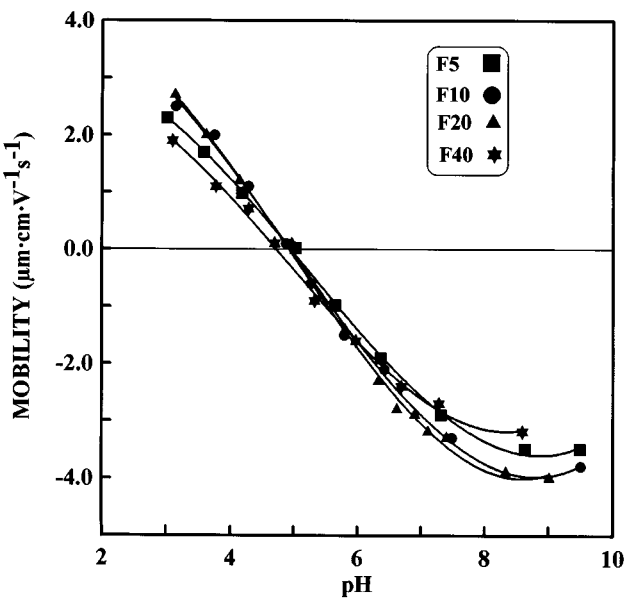

FIG. 8. Electrophoretic mobilities measured as a function of pH for $Fe/ZrSiO_4$ samples heated at 1200°C and leached.

CONCLUSIONS

Reddish iron zircon pigments of various hues can be prepared by heating at different temperatures (from 1000 to 1200°C) amorphous precursors obtained by pyrolysis of a liquid aerosols with the zircon composition and variable iron contents. These powders consist of spherical particles with diameter ranging from 20 to 200 nm. The crystallization of zircon took place on heating at lower temperatures in the pigments (1000°C) than in undoped zircon (1400°C), not requiring the use of mineralizing agents. This behavior is explained by the presence of a solid solution between Fe^{3+} cations and tetragonal zirconia, which would favor the diffusion process involved in the zircon formation. The color of the iron zircon pigments is ascribed to homogeneously distributed α-Fe_2O_3 particles in the zircon matrix.

ACKNOWLEDGMENTS

This work has been supported by the Comisión Interministerial de Ciencia y Tecnología under projects MAT92-0328 and MAT95-0947-E. P.T. acknowledges a fellowship of Ministerio de Educacion y Ciencia. We thank Dr. Mercedes Gracia and Dr. Agustín Rodríguez for their help in recording the Mössbauer and XPS spectra, respectively.

REFERENCES

1. B. T. Bell, *Rev. Prog. Coloration* **9,** 48 (1978).
2. M. S. Bibilashvili, O. S. Grum-Grzhimailo and N. S. Belostotskaya, *Ceram. Int.* **9,** 142 (1983).
3. M. Trojan, *Dyes Pigments* **13,** 177 (1990).
4. F. J. Berry, D. Eadon, J. Holloway, and L. E. Smart, *J. Mater. Chem.* **6,** 221 (1996).
5. E. Matijevic, *Langmuir* **2,** 12 (1986).
6. M. Ocaña, J. Sanz, T. González-Carreño, and C. J. Serna, *J. Am. Ceram. Soc.* **76,** 2081 (1993).
7. P. Tartaj, J. Sanz, C. J. Serna, and M. Ocaña, *J. Mater. Sci.* **29,** 6533 (1994).
8. G. L. Messing, S. Zhang, and G. V. Jayanthi, *J. Am. Ceram. Soc.* **76,** 2707 (1993).
9. T. González-Carreño, A. Mifsud, C. J. Serna, and J. M. Palacios, *Mater. Chem. Phys.* **76,** 2081 (1991).
10. P. Tartaj, J. Soria, C. J. Serna, and M. Ocaña, *J. Mater. Res.* (in press).
11. P. Tartaj, C. J. Serna, and M. Ocaña, *J. Am. Ceram. Soc.* **78,** 1147 (1995).
12. J. Rodriguez-Carvajal, "Abstracts of the Satellite Meeting on Power Diffraction of the XV Congress of the International Union of Crystallography," p. 127. Toulouse, 1990.
13. J. E. Post and D. L. Bish, "Reviews in Mineralogy" (D. L. Bish and J. E. Post, Eds.), Vol. 20, p. 288. Mineralogical Society of America, Washington, 1989.
14. K. Robinson, G. N. Gibbs, and P. H. Ribbe, *Am. Mineral.* **56,** 782 (1971).
15. G. Teufer, *Acta Crystallogr.* **15,** 1187 (1962).
16. *Nat. Bur. of Stand., Monogr.* (*U.S.*) **25,** 13 (1976).
17. M. Ocaña, V. Fornés, and C. J. Serna, *J. Non-Cryst. Solids* **107,** 187 (1989).
18. M. Ocaña, V. Fornés, and C. J. Serna, *Ceram. Inter.* **18,** 99 (1992).
19. ASTM Card 27-997.
20. ASTM Card 42-1164.
21. T. González-Carreño, P. Tartaj, J. Sanz, C. J. Serna, and M. Ocaña, *Adv. Sci. Technol.* **3B,** 1211 (1995).
22. C. Pecharromán, M. Ocaña, P. Tartaj, and C. J. Serna, *Mater. Res. Bull.* **29,** 417 (1994).
23. C. J. Serna, M. Ocaña, and J. E. Iglesias, *J. Phys. C* **20,** 473 (1987).
24. S. Davison, R. Kershaw, K. Dwight, and A. Wold, *J. Solid State Chem.* **73,** 47 (1988).
25. F. J. Berry, M. H. Loretto, and M. R. Smith, *J. Solid State Chem.* **83,** 91 (1989).
26. M. V. Tsodikov, O. V. Bukhtenko, O. G. Ellert, V. M. Shcherbakov, and D. I. Kochubey, *J. Mater. Sci.* **30,** 1087 (1995).
27. P. Tartaj, J. S. Moya, J. Requena, S. de Aza, F. Guitían, C. J. Serna, and M. Ocaña, *J. Mater. Sci.* **31,** 6089 (1996).
28. W. Kundig, H. Bömmel, G. Constabaris, and R. H. Lindquist, *Phys. Rev.* **142,** 327 (1966).
29. R. J. Armstrong, A. H. Morrish, and G. A. Sawatzky, *Phys. Lett.* **23,** 415 (1966).
30. M. F. Thomas and C. E. Johnson, "Mössbauer Spectroscopy" (P. E. Dickson and F. J. Berry, Eds.), Chap. 6. Cambridge University Press, Cambridge, 1986.
31. A. J. Koch and J. J. Becker, *J. Appl. Phys.* **39,** 1261 (1968).
32. C. D. Wagner, W. H. Riggs, L. E. Davis, J. F. Moulder, and G. E. Muilinberg, "Handbook of X-Ray Photoelectron Spectroscopy." Perkin-Elmer Corporation, Minnesota, 1973.
33. C. D. Wagner, D. E. Passoja, H. F. Hillery, T. G. Kinisky, H. A. Six, W. T. Jansen, and J. A. Taylor, *J. Vac. Sci. Technol.* **21,** 933 (1982).
34. M. Mao, D. Fornasiero, J. Ralston, R. St. C. Smart, and S. Sobieraj, *Colloids Surf. A* **85,** 37 (1994).
35. E. Matijevic and P. Scheiner, *J. Colloid Interface Sci.* **63,** 509 (1978).
36. G. A. Parks, *Chem. Rev.* **65,** 177 (1965).
37. M. Kerker, P. Scheiner, D. D. Cooke, and J. P. Kratohvil, *J. Colloid Interface Sci.* **71,** 176 (1979).